# Beating of hemp bast fibres: an examination of a hydro-mechanical treatment on chemical, structural, and nanomechanical property evolutions

Justine Padovani, David Legland, Miguel Pernes, Antoine Gallos, Céline Thomachot-Schneider, Darshil U. Shah, Alain Bourmaud, Johnny Beaugrand

## HAL Id: hal-02627443
## https://hal.inrae.fr/hal-02627443

# Beating of hemp bast fibres: an examination of a hydro-mechanical treatment on chemical, structural, and nanomechanical property evolutions

JUSTINE PADOVANI[1], DAVID LEGLAND[2], MIGUEL PERNES[1], ANTOINE GALLOS[3], CÉLINE THOMACHOT-SCHNEIDER[4], DARSHIL U. SHAH[5], ALAIN BOURMAUD[6], JOHNNY BEAUGRAND[1,2]*

[1] FARE Laboratory, INRA, Université de Reims Champagne-Ardenne, 2 Esplanade Roland-Garros, 51100 Reims, France

[2] Biopolymères Interactions Assemblages (BIA), INRA, Rue de la Géraudière, 44316 Nantes, France

[3] URD Agro-Biotechnologies Industrielles (ABI), AgroParisTech, CEBB, 3 rue des Rouges Terres, F-51110 Pomacle, France

[4] Groupe d'Etudes sur les Géomatériaux et les Environnements Naturels, Anthropiques et Archéologiques (GEGENAA, EA 3795), Université de Reims Champagne-Ardenne, Reims, France

[5] Department of Architecture, Centre for Natural Material Innovation, University of Cambridge, Cambridge, CB2 1PX United Kingdom

[6] Université de Bretagne Sud, UMR CNRS 6027, IRDL, F-56100 Lorient, France

**\*Corresponding author: johnny.beaugrand@inra.fr**

## Abstract

In this study, a gradually increased hydro-mechanical treatments duration were applied to native hemp bast fibres with a traditional pulp and paper beating device (laboratory Valley beater). There is often a trade-off between the treatment applied to the fibres and the effect on their integrity. The multimodal analysis provided an understanding of the beating impact on the fibres at multiple scales and the experimental design made it possible to distinguish the effects of hydro- and hydro-mechanical treatment. Porosity analyses showed that beating treatment doubled the macroporosity and possibly reduced nanoporosity between the cellulose microfibrils. The beating irregularly extracted the amorphous components known to be preferentially located in the middle lamellae and the primary cell walls rather than in the secondary walls, the overall increasing the crystallinity of cellulose from 49.3 % to 59.1 %, but a non-significant change in the indentation

34 moduli of the cell wall was observed. In addition, <mark>beating</mark> treatments with two distinct mechanical

35 severities showed a disorganization of the cellulose conformation, which significant dropped the

36 indention moduli by 11.2 GPa and 8.4 GPa for 10 and 20 minutes of Valley beater hydro-

37 mechanical treatment, respectively, compared to hydro-treated hemp fibres (16.6 GPa). Pearson's

38 correlation coefficients between physicochemical features and the final indentation moduli were

39 calculated. Strong positive correlations were highlighted between the cellulose crystallinity and

40 rhamnose, galactose and mannose as non-cellulosic polysaccharide components of the cell wall.

41

## Keywords

43 *Pile Valley <mark>beater,</mark> Plant cell wall, Nanoindentation, Porosity, Biochemistry,*

44 *Natural fibre processing*

45

## Abbreviations

47 DVS:                                      dynamic vapour sorption;

48 HPAEC-PAD:                    high-performance anion-exchange chromatography with
49                                             pulsed amperometric detection;

50 HPLC:                                   high-performance liquid chromatography;

51 MFA:                                     microfibrillar angle;

52 MIP:                                      mercury intrusion porosimetry;

53 <mark>NCP's:                                 non cellulosic polysaccharides</mark>

54 SEM:                                     scanning electron microscopy;

55 XRD:                                     X-ray diffraction

56

## INTRODUCTION

58 Lignocellulosic fibres have been of increasing interest in recent years in the field of

59 agromaterials (Gallos et al. 2017). Their good mechanical properties make them a

60 potential candidate to replace conventional man-made reinforcements in composite

61 materials (Bourmaud et al. 2018; Mohanty et al. 2018; Wambua et al. 2003). Due

62 to their multi-scale hierarchical structure, lignocellulosic fibres are akin to

63 composite materials (Bourmaud et al. 2018). In plants, fibres are organized in

64 bundles comprising several elementary fibres. Elementary fibres consist of a cell

65 wall made mostly of cellulose (β-linked glucose unit chains) in a semi-crystalline

66  state (Turner and Kumar 2018). Cellulose microfibrils are parallel to each other,

67  forming a microfibrillar angle (MFA) with the cell axis, and a fraction of them are

68  connected to non-cellulosic matrix, usually called amorphous, made of

69  hemicelluloses (mainly xyloglucan), pectins such as homogalacturonan (Morvan et

70  al. 2003) and a small amount of lignins.

71  The cell wall of elementary lignocellulosic fibres is organized in concentric layers:

72  from the outermost to the innermost, we find the primary cell wall; the secondary

73  cell wall is composed of a xylan-rich layer type which is located on the outer

74  periphery of a gelatinous layer type (also called S2); and finally a central lumen.

75  The elementary fibres are linked together thanks to the pectic-rich middle lamella.

76  The gelatinous layer type has a high cellulose content (80-90 %), high crystallinity

77  index, and low angle of cellulose microfibrils, and in the case of hemp primary

78  fibres, it is the thickest layer of the cell wall, more than 10 µm (Chernova et al.

79  2018).

80  Hemp bast fibres are used as composites in different industries, notably because

81  hemp's cell wall is thick, with a reduced lumen (Beaugrand et al. 2017; Placet et al.

82  2014), which gives it a high coarseness and is assumed to be non-collapsible

83  (Westenbroek 2000). Hemp bast fibres are generally composed of 53-91 %

84  cellulose, 4-18 % hemicelluloses, 1-17 % pectins, 1-21 % lignins in dry matter (Liu

85  et al. 2017) and a low amount of wax present in the middle lamella (Thygesen et al.

86  2006a). The large disparity in reported chemical composition can be explained by

87  the fact that the analyses were not carried out at the same stage of fibre maturity or

88  with the same measurement protocol (Bourmaud et al. 2018).

89  The mechanical properties of the cell walls are governed by several factors, such as

90  the microfibrillar angle (Burgert and Keplinger 2013), the chemical composition

91  (Lefeuvre et al. 2014), the crystallinity, the defect density (Andersons et al. 2009;

92  Beaugrand and Guessasma 2015; Gourier et al. 2017; Hughes 2012; Guessasma and

93  Beaugrand 2019) and the mesoporosity (pore size between 2 and 50 nm), even if

94  the last factor is not yet well established at the elementary fibre scale. Arnould et

95  al. (2017) mapped the stiffness of the cell wall of green flax stems by atomic force

96  microscopy revealing a gradient in mechanical properties along the cross section at

97  nanoscale. However, this gradient in properties is not observed in mature plants,

98  except in cases of environmental accident, such as drought or lodging events.

99  The mechanical properties of short lignocellulosic fibre–reinforced thermoplastic

100  composite materials are inherent to the properties of the fibres that make them up

101  (Bourmaud et al. 2018; Shah 2013; Shah et al. 2016), including such variables as

102  their reinforcement rate (Ausias et al. 2013), their orientation in the matrix (Tanguy

103  et al. 2018), their defects (Beaugrand et al. 2017; Rask et al. 2012), their shape

104  (Beaugrand and Berzin 2012; Berzin et al. 2014; Legland and Beaugrand 2013) and

105  the fibre-polymer matrix adhesion (Le Moigne et al. 2018). However,

106  lignocellulosic fibres are hydrophilic, i.e., they easily adsorb water molecules. This

107  property, incompatible with the hydrophobic character of some thermoplastic

108  matrices, such as polyolefins, can be a barrier to good fibre-matrix adhesion in

109  composite materials. Many researchers have conducted work to improve fibre-

110  matrix adhesion by applying thermal, mechanical and/or chemical pre-treatments

111  to plant fibres. Numerous efforts to improve the properties of composites have been

112  reviewed. Pickering et al. (2016) provide a synthesis of the various factors affecting

113  the mechanical properties of natural fibre composites. More recently, Liu et al.

114  (2017) reported the effects of many targeted pre-treatment techniques on hemp bast

115  fibres intended for composite application.

116  Among the existing processes, the beating process is traditionally used in the pulp

117  and paper industry. The effects of this treatment on wood are well known and

118  described by Gharehkhani (2015), whereas much less knowledge is available on

119  lignocellulosic plant fibres. The main ones are internal and external fibrillation -

120  and consequently the opening of pore structure, increasing their swelling capacity -

121  and the breakage and the straightening of the macrofibrils. However, also their

122  chemical composition is changed by degumming cellulosic fibres, i.e., beating

123  cellulose by removing the non-cellulosic fraction. To control the quality of the pulp,

124  pulp and paper standard methods of characterization are used, such as the Schopper-

125  Riegler degree (Dienes et al. 2005) or the water retention value (Cheng et al. 2010).

126  Moreover, nanocelluloses are increasingly attracting materials science researchers

127  and are being incorporated into formulations, and mechanical characterization

128  techniques are applied to assess the properties of the fibres.

129  We tried to increase the external surface area of the hemp fibre elements by

130  individualizing the bundles and producing microfibrils. To do this, we developed a

131  soft hydro-mechanical treatment using a Valley beater. The effects of the treatment

132  were revealed by analyses of the structural, chemical and nanomechanical features

obtained by SEM observations, polysaccharide analysis, porosity, cellulose XRD crystallography and nanoindentation. Process impacts were depicted on the fibres' structure and therefore on their mechanical properties. Finally, a correlation study identified the parameters that had the greatest impact on the nanomechanical properties of the fibres.

## MATERIALS AND METHODS

*Plant materials*

The native fibres used for this study were whole-plant hackled non-retted hemp fibres (*Cannabis sativa L.* variety Fedora 17). Hemp was cultivated and harvested in Champagne-Ardenne (France, 2012) and cut to an average length of 15 millimetres by Fibres Recherche Développement (FRD, Troyes, France). Samples were stored in a dark environment at ambient temperature and humidity.

*Beating and drying of hemp fibres*

Before beating, hemp fibres were water-soaked for 10 min in a laboratory pulper at ambient temperature to clean them and remove any impurities. For this, 400 g of hemp fibre was immersed in 4 l of water (10 % w/v consistency) and stirred at a low rotational speed (510 rpm). Then, the cloudy water was removed and the bulk fibres put into the Valley beater (described in TAPPI 200) container. The container was then topped off with water to obtain a 2 % w/v consistency. The device was turned on for 5 minutes without counterweight to homogenize the suspension. The beating process started right after a weight of 4 kg was fixed to the lever arm which corresponds to applying a force of 76.3 N upwards against the roll. The rotational speed of the roll was 510 rpm and the cutted edge length (CEL) calculated from Eq.1 was 34.7 m.r$^{-1}$. From these two parameters and Number of crossing points ($N_{cp}$) (Eq.2) between the roll and bedplate bars, we determined the cumulative number of crossing points ($CN_{cp}$) per beating time (Table 1). All experiments were conducted with the same fibre concentration, counterweight and soaking time, only the beating time changes.

$$CEL = \frac{n_r.n_s.l_0}{\cos \alpha_R.\cos \alpha_S} \tag{1}$$

$$N_{CP} = \frac{CEL}{\pi.D_R}.\sin (\alpha_R + \alpha_S) \tag{2}$$

5

169

170 The unbeaten native hemp fibres were the "ubH" sample, the beaten 0 minute hemp
171 fibres (only hydro-treated as hydro treatment) were the "bH_0" sample, the hydro-
172 beaten 10 minutes hemp fibres were the "bH_10" sample, and finally, the hydro-
173 beaten 20 minutes hemp fibres were the "bH_20" sample (as the hydro-mechanical
174 treatment).

175

176 Table 1: Experimental design

| Type | Code | Soaking time (min) | Beating time (min) | $CN_{cp}$ | SR° |
|---|---|---|---|---|---|
| Fibre consistency (w/v) | - | 10% | 2% | - | |
| Un-beaten hemp fibres (raw material) | ubH | 0 | 0 | 0 | n.a. |
| beaten 0 min Hemp fibres | bH_0 | 10 | 0 | 0 | $7 \pm 0.3$ |
| beaten 10 min Hemp fibres | bH_10 | 10 | 10 | $1.6\ 10^6$ | $8 \pm 0.4$ |
| beaten 20 min Hemp fibres | bH_20 | 10 | 20 | $3.2\ 10^6$ | $12 \pm 0.4$ |

177

178

179 The beaten fibre suspension was filtered on a homemade system made of a nylon
180 net having a pore size of 200 µm that was attached to a wooden stretcher frame of
181 690×420 mm, i.e., a total surface area of 0.29 m² per frame. The frame was placed
182 in a large stainless-steel industrial sink. The suspension was spilled on it, and the
183 fibres were manually dispersed on a nylon net surface to keep them as separate as

6

184 possible. After that, the water was evacuated, and the nylon net surface was put
185 inside a ventilated oven at 30 °C for 2 hours.

186 *Schopper-Riegler degree (SR°)*

187 This rate is an indicator of the degree of beating of a fibrous suspension based on
188 its ability to drain water that results directly from its surface conditions (fibrillation)
189 and the swelling of the fibres. Thus, the higher the Schopper-Riegler degree, the
190 more the pulp retains water and is more beaten. Unlike classical pulp, in this study
191 hemp fibres were beaten with a shorter duration than typical paper making time, in
192 order to maintain maximum integrity and mechanical properties. Therefore, to have
193 a denser fibre mat, a suspension of 4 g of dry fibres (rather than 2 g) was diluted in
194 1 l of water and introduced into the fill chamber of freeness tester. The water content
195 of the suspension passed through a wire screen that retained the fibres and formed
196 a mat. In the funnel, if the flow speed was too fast, the drained water exited by the
197 lateral orifice and discharged in the corresponding graduated measuring cylinder.
198 After a drying step, the absolute fibre mat mass was weighed to correct the SR° to
199 2 grams per litre absolute dry weight. The SR° value of each treated fibre lot was
200 averaged across 4 tests (Table 1).

201 *Scanning electron microscopy*

202 The surface appearance of the unbeaten and beaten fibres bundles was observed
203 with a table-top scanning electron microscope (Hitachi TM-1000). This equipment
204 did not require coating the fibres, and SEM images were taken at a magnification
205 of 200 times and at an accelerating voltage of 15 kV.

206 *Chemical composition*

207 The glyosidic linkages of polysaccharides were hydrolysed by two-step sulphuric
208 acid attack to release monosaccharides and uronic acids. To open the structures, 10
209 milligrams of milled fibres (sieved of 200 µm) was mixed with 125 µl of $H_2SO_4$ 12
210 M under stirring at room temperature for 2 hours, corresponding to the swelling
211 step. Then, the $H_2SO_4$ concentration was lowered by dilution at 1 M, and the
212 mixture was heated at 100 °C for 2 hours to achieve the total hydrolysis.

7

Monosaccharides were separated and quantified by high-performance anion-exchange chromatography equipped with CarboPac Pa-1 Column. The detailed procedure was previously described by Herbaut (2018).

Cellulosic material is considered the sum of glucose (Glc), whereas the non-cellulosic polysaccharides (NCPs) content is the sum of the monomer units: arabinose (Ara), rhamnose (Rha), galactose (Gal), xylose (Xyl), mannose (Man), galacturonic acid (Gal Ac) and glucuronic acid (Glc Ac).

The acid-insoluble lignin content was quantified as described previously (Sharma et al. 2018). Milled samples (200 mg) were submitted to acid hydrolysis by mixing with 2 ml of a 12 M $H_2SO_4$ solution for 2 h at room temperature. The acid solution was then diluted to a concentration of 2 M by addition of deionized water before an incubation of 3 h at 100 °C. The solid fraction was recovered, thoroughly washed and oven-dried at 105 °C to a constant weight. The Klason lignin content was calculated after correction for ash content, which was determined by calcination at 550 °C for 4 h.

The protein content was estimated from the nitrogen content of the fibres. Experiments were carried out using a EURO EA elemental analyser (Eurovector, Milan, Italy) equipped with a thermal conductivity detector. A precise mass of approx. 5 to 7 mg of dried-milled samples was weighed in a tin capsule, then hermetically sealed. Based on the Dumas method (Dumas 1831), the samples were fully flash-combustion oxidized, and nitrogen was converted into gaseous dinitrogen ($N_2$). A correction factor (x6.25) was applied to nitrogen content to estimate the protein content (González López et al. 2010).

*Hygroscopic properties by dynamic vapour sorption*

The isotherms of the water vapour desorption/adsorption were determined using a dynamic vapour sorption (DVS) apparatus from Hiden Isochema Ltd. (UK). Nearly 5 mg hemp fibres was placed into the microbalance's stainless-steel basket (precision of 0.1 µg), then placed hermetically in a double-jacket reactor connected to a thermoregulated water bath and equipped with temperature and relative humidity (RH) sensors to monitor them. Relative humidity was obtained with a flow mixture of wet and dry nitrogen. Once the sample was loaded into the DVS apparatus, the sorption/desorption sequence was started (10 % to 90 %RH then back to 10 %RH with a 10 % step) at a constant and regulated temperature of 20°C. Then,

246 a drying sequence was programmed to obtain the dry mass of the sample (4 h at 40

247 °C then 8 h at 20 °C, under a flow of dry nitrogen). More details on the procedure

248 are given by Guicheret-Retel (Guicheret-Retel et al. 2015). The moisture uptake

249 was calculated as follows (Eq. 3) using the mass measured at the equilibrium

250 moisture content for chosen RH ($m_{moist}$)and the mass of dried sample ($m_{dry}$)

251 $$\omega\ (\%) = \frac{m_{moist} - m_{dry}}{m_{dry}} \times 100 \tag{3}$$

252

### True Density

254 True density measurements were carried out using the DVS apparatus from Hiden

255 Isochema Ltd. (UK). Argon was used because it is an inert and heavy gas.

256 Approximately 60 mg samples were used. The principle of this technique is to

257 measure the apparent mass of the sample as a function of the pressure of argon

258 applied from 1 to 10 bars with an interval of 1 bar. We obtained a linear curve of

259 10 aligned points from which the slope was extracted and used to calculate the

260 density of the sample using the buoyancy equation.

261 Before any measurement, a purge and dry cycle of the sorption microbalance was

262 performed to obtain 100 % argon in the DVS device and to have a dried sample. To

263 this end, we injected argon and put the system under vacuum approximately 20

264 times, and then we maintained the sample under vacuum until its mass was constant.

### Fibre diameter distribution

266 The fibre diameters were measured by a high-resolution 2D scanner (Epson V850

267 pro) by scattering them on the scanner glass and taking care to keep them

268 individualized. The images were acquired in 8-bit greyscale at a resolution of 4800

269 dpi representing theoretically 5.29 µm per pixel. The images were processed and

270 analysed with ImageJ software. After a manual segmentation step by setting a

271 threshold value, the fibres were labelled using the "binaryLabel8" plugin. The

272 length of the fibres was obtained by computing their geodesic diameter, as

273 implemented in the "MorphoLibJ" plugin (Legland et al. 2016; Legland and

274 Beaugrand 2013). Their diameter was obtained from the largest circle that could be

275 contained in the fibre. To plot the diameter distribution graphic, particles with a

276 length strictly less than 200 µm were excluded by numerical threshold. Also, by

277 convention, they are considered as 'fine' elements and not fibres (Ferreira et al.
278 1999).

*Thermogravimetric analysis*

280 Thermogravimetric analysis was performed on TGA Q800 (TA instruments Inc,
281 USA) with a nitrogen flow (40 ml.min$^{-1}$) from 25 °C to 1000 °C and a temperature
282 ramp of 10 °C·min$^{-1}$. The analysis was performed on approximatively 20 mg of
283 powder fibres (200 µm).

*Mechanical properties of the cell wall*

285 The mechanical properties were assessed by nanoindentation. This technique
286 requires the samples to be embedded in a resin. Before this step, the cell wall
287 structure of hemp bundles was fixed using a paraformaldehyde (2 %)–
288 glutaraldehyde (0.5 %) solution for 2 hours at room temperature. The fixed sample
289 was dehydrated by successive ethanol solution baths (20 min) of increasing
290 concentration until absolute grade. The samples were then soaked in successive
291 solutions of ethanol/resin with an increasing ratio of resin until 100 % of resin.
292 During those steps, the ethanol was gradually and then totally substituted by the LR
293 White resin (Sigma-Aldrich). After that, the samples were placed inside a specific
294 gelatine capsule and put in an oven. Finally, the resin polymerization was
295 performed for 24 hours at 60 °C.
296 The LR White capsule was cut in the transversal axis of the hemp bundles, and the
297 excess resin around the fibre was manually removed. An ultra-microtome (Microm
298 Microtech, HM 360) equipped with a diamond knife was used to smooth the sample
299 surface and to obtain a roughness below 0.5 µm.
300 A Nanoindenter Xp equipped with a pyramidal indenter (Berkovich tip) was used
301 to perform indentation measurements. The Nanoscope Analysis software enabled
302 us to extract the indentation modulus and the indentation hardness from the load-
303 unload curve of the specimen according to the method described by Oliver-Pharr
304 method (Oliver and Pharr 1992). The indentation method parameters were fixed as
305 follows: the maximum depth was 120 nm; the loading rate was 1 µN·s$^{-1}$; the dwell
306 time at the maximum load was 20 s and the unloading rate was 10 µN·s$^{-1}$.

307 *X-ray crystallography*

308 An ultra-centrifugal mill (Retsch ZM 200) was used to grind the hemp fibres to
309 approximately 200 microns in length. The samples were scanned from $2\theta = 5$ to $40$
310 $^\circ$ with a step size of $0.03\,^\circ$ at $2\ \text{s}\cdot\text{step}^{-1}$ at $30\,\text{kV}$ and $20\,\text{mA}$ under ambient conditions
311 on a Siemens D500 diffractometer using CoK$\alpha$ radiation. The crystallinity index
312 was calculated using Eq. 4 according to the Segal empirical method (Segal et al.
313 1959):

314 $$C = \frac{I_{tot} - I_{am}}{I_{tot}} \times 100 \tag{4}$$

315 where $I_{tot}$ is the intensity at the primary peak for cellulose I (at $2\theta = 22.5\,^\circ$) and $I_{am}$
316 is the intensity from the amorphous portion evaluated as the minimum intensity (at
317 $2\theta = 18.5\,^\circ$) between the primary and the secondary peaks.

318 *Mercury intrusion porosimetry*

319 To determine the pore size distribution and the total pore volume, an Autopore IV
320 9500 (Micrometrics) was used. Approximatively 150 mg of dried fibres were
321 loaded in a suitable penetrometer. This technique is based on the non-wetting
322 property of liquid mercury having high a surface tension ($\gamma = 480$ dyne/cm at 20°C)
323 and a high contact angle ($\theta$air/mercury $= 140°$) on many surfaces. The mercury was
324 gradually injected into the porous network thanks to an increasing pressure from
325 0.003 MPa (178 μm) to 227 MPa (0.003 μm). The pore access (r) invaded, which
326 was determined by the Washburn equation (Washburn 1921), is inversely
327 proportional to the exerted pressure (Eq. 5).

328 $$r = \frac{-2\gamma cos\theta}{P} \tag{5}$$

329 *Statistical analysis*

330 For chemical analyses, nanomechanical properties and true density measurements,
331 the equality of variance (Fisher test) was verified. Student's t-test was carried out
332 to compare the samples by pair, with a significance level of probability set at $p <$
333 0.05. Pearson's correlation coefficients were evaluated between indentation moduli
334 and chemical analyses, with a statistically significant p-value of $< 0.05$, using
335 SigmaPlot 12.0 software (Systat Software, Chicago, USA).

336

## RESULTS AND DISCUSSION

*Structural changes*

The fibre suspensions were first characterized by the Schopper–Riegler test, which shows the progress of beating by the ability of the fibres to drain water. The beaten fibres had a SR° of 8 and 12 for bH_10 and bH_20 respectively (Table 1). This increase compared to water-soaked fibres (bH_0) clearly showed that the fibre structure had been modified by mechanical beating, and the longer the beating, the greater the extent of modification.

Moreover, microscopic observations were conducted to visualize the fibre elements structural and topological natives state (ubH) and induced changes undergone by the hydro (bH_0) and hydro-mechanical treatments (bH_10 and bH_20). The resulting images are shown in Figure 1. Untreated fibres (ubH) were thicker and had a rougher surface. After treatment, the surface of the fibres seemed to be cleaner, smoother but also finer and more defibrillated, especially with longer pretreatment times. The surface cleaning of fibre by an immersion step is long, and here our observations mostly confirm this. More interestingly, mechanical treatment (bH_10 and bH_20) resulted in defibrillation: the bundles dissociated into thinner fibres, and the upper layers of the fibres in the cell wall give rise to external fibrils or to fine particles if they dissociated from them. These phenomena are well known for wood (Gharehkhani et al. 2015; Page 1989) and for hemp (Wang et al. 2007). In line with enhanced plant fibre composite mechanical properties, especially for short-fibre thermoplastic composites, the physical anchoring in the matrix mediated by fibrillation harboured by natural fibres is one promising route (Lee and Bismarck 2014; Zhong et al. 2011). One goal of this study was to generate such lateral fibrils along the fibres (see arrow in Figure 1), and the microscopic observations confirm the effectiveness of the Valley beater hydro-mechanical treatment.

364
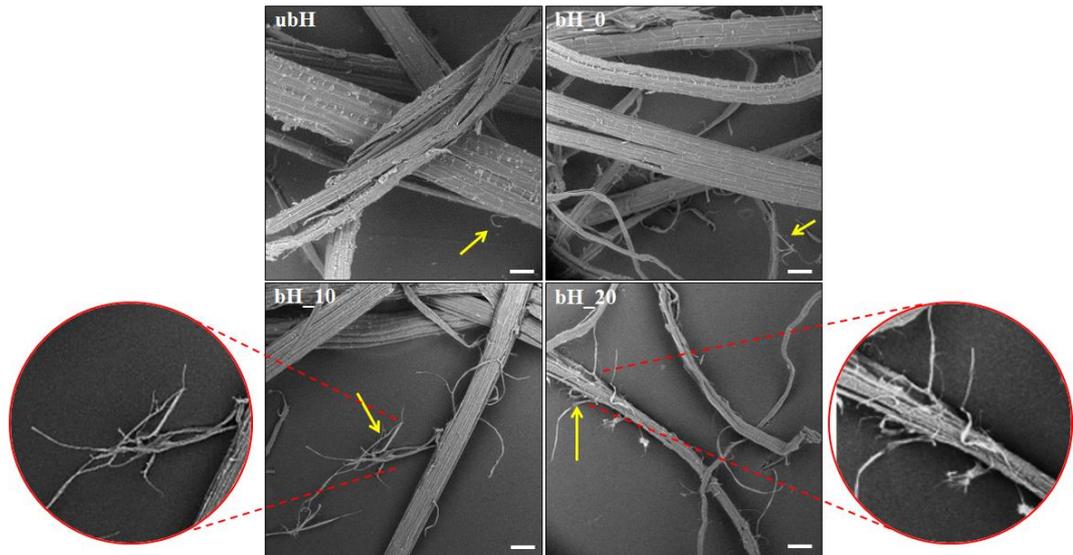
Figure 1: SEM micrographs. White scale bar equal to 50 µm. Yellow arrows point the lateral
microfibrils more or less visible and amplified depending on the treatment severity.

Further details about the evolution of the morphologies were obtained by image analysis. The average diameters of nearly 600 fibres with a minimum length of 200 µm were measured for each sample to have a global representation of the fibre population (Figure 2). The majority of the untreated fibres (ubH) extend to diameters between 20 and 60 µm. The same trend was observed for water-soaked fibres (bH_0), with a slight enrichment of this fraction, suggesting that the soaking step has allowed the beginning of individualisation of some bundles. This would be in agreement with the water-soluble non-cellulosic polymers extracted from the fibre elements, in particular from the middle lamella that 'glued' the elementary fibre together. This range was gradually reduced to 20-40 µm for mechanically treated fibres with a 50 % enrichment compared to native fibres (ubH). As the fibres were beaten as the mechanical treatment progresses, these diameter results corroborated the abovementioned microscopic observations. It should be noted that the method of measuring the diameter by the largest inscribed circle that can be contained in the fibre may slightly overestimate the diameter, especially for the most fibrillated fibres. Indeed, we noticed that this larger inscribed circle tended to be at the branching points.
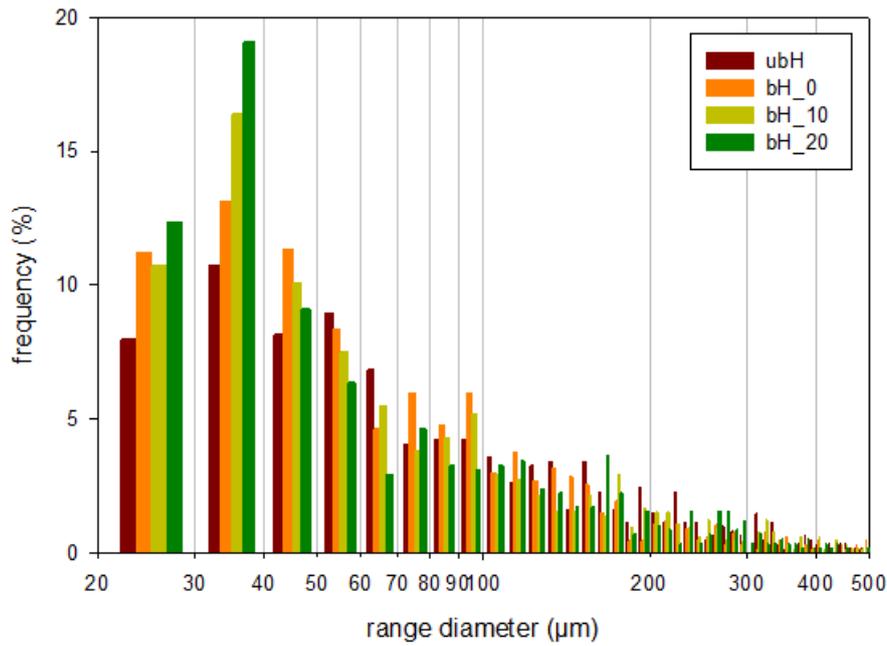
385

386    Figure 2: Diameter distributions of hemp fibres greater than 200 µm in length.

387

## Porosity and swelling

389    With the objective to estimate the impact of soaking and beating on the porous

390    structure and surface pore area of hemp fibres, a porosity analysis was performed

391    by mercury intrusion porosimetry (MIP). The mercury porosity obtained on the

392    native fibres (ubH) was 49.8 %. In the water-soaked fibres (bH_0), the porosity

393    was higher with a value of 62.6 %. The total porosity increased with the mechanical

394    treatment applied to the fibres (64.8 % for bH_10 and 83.3 % for bH_20).

395    Regarding the pore distribution (Figure 3A), the mean pore access for the native

396    fibres was approximately 75 µm that corresponded to the interfibre spaces.
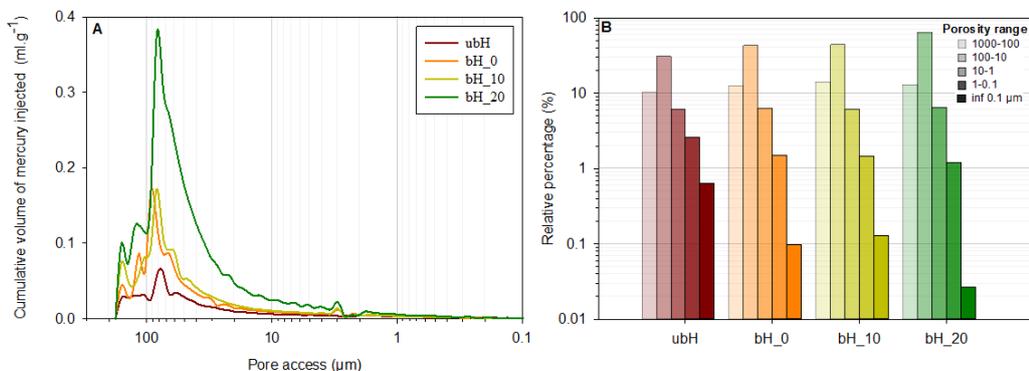


397

398 Figure 3: Incremental volume of mercury injected as a function of pore access (µm) (3A) and
399 range of porosity distribution in relative percentage for each fibre sample (3B). The legend of the
400 Figure 3B shows the intensity gradient corresponding to each porosity range.

401

402 This mean pore access was up to 90 µm for the water-soaked fibres and up to 83
403 microns for the mechanically treated fibres. A small peak approximately 3 µm
404 which intensity increased with the treatment constituted the fibres microporosity
405 could correspond to the lumens. They were defined as hollow and elongated
406 cavities with transversal diameter between 0.5-10 µm (Del Masto et al. 2017; Placet
407 et al. 2014). This observation obtained with the MIP also matches well with the
408 lumen description visualized by X-ray nanotomography (Beaugrand et al. 2017).
409 Considering the relative percentages of the pore access ranges (Table 2), we can
410 see that it was the 10-100 µm range that increased significantly, i.e., it increased
411 by 30 % for bH_0 and bH_10 and almost doubled for bH_20 compared to native
412 fibres.

413 Table 2: Mercury intrusion porosimetry results: total porosity and apparent skeletal density. True
414 density obtained by DVS. True densities not having the same letter were significantly different
415 (p<0.05).

416

|  | Total porosity (%) | Apparent skeletal density (g·ml$^{-1}$) | True density |
|---|---|---|---|
| ubH | 49.8 | 1.379 | $1.535 \pm 0.004$[a] |
| bH_0 | 62.6 | 1.280 | $1.541 \pm 0.004$[a] |
| bH_10 | 64.8 | 1.254 | $1.534 \pm 0.005$[a] |
| bH_20 | 83.3 | 1.453 | $1.550 \pm 0.004$[a] |

417

418 This reflects the densification of porous networks, both intrafibre and interfibre,
419 through bundle individualization and the formation of lateral microfibrils that can
420 become entangled and sometimes in loops as can be observed in the SEM images
421 (Figure 1). Pores smaller than 0.1 microns almost completely disappeared as soon
422 as the fibres were soaked and dried. These nanopores corresponded to the pores
423 between the microfibrils (Meng and Ragauskas 2014), so the soaking/drying cycle
424 imposed on the fibres tightened the cellulose microfibrils between them.

In addition, water sorption tests using DVS were conducted to learn about the qualitative evolution of mesoporosity. Indeed, in the case of natural fibres, a hysteresis was observed during the desorption phase, reflecting the presence of mesopores in the fibre structure (Célino et al. 2013; Hill Callum et al. 2009). Recently, Chen et al. (2018) have provided, through simulations, a better understanding of the role of hydrogen bonds involved in the hysteresis observed in sorption-induced swelling of soft nanoporous polymers.

The isotherms were analysed by two means: (i) the loop isotherm area (Table 3) resulting from subtraction of the desorption curve area from the sorption curve area (Figure 4A), for which areas were estimated by the trapezoidal rule; and (ii) the hysteresis curves, i.e., the difference in water uptake (ω) between desorption point and sorption point as a function of relative humidity (Figure 4B).

Table 3: Characterization results of untreated and treated hemp fibres: (i) loop area of the sorption/desorption curve, (ii) nanoindentation modulus and (iii) crystallinity. Values not having the same letter were significantly different ($p < 0.05$).

| | Loop area ($\omega\%\cdot$RH%) | Total sugar content (%dry matter) | Crystallinity (%) | Indentation modulus from unload (GPa) |
|---|---|---|---|---|
| ubH | 75.2 | $84.3 \pm 7.6^a$ | 49.3 | $15.1 \pm 2.7^a$ |
| bH_0 | 86.1 | $86.5 \pm 4.2^a$ | 59.1 | $16.6 \pm 2.5^a$ |
| bH_10 | 94.4 | $85.1 \pm 3.1^a$ | 56.6 | $11.2 \pm 1.0^b$ |
| bH_20 | 91.7 | $91.5 \pm 2.3^b$ | 54.1 | $8.4 \pm 1.0^c$ |

Water sorption and desorption isotherms are shown in Figure 4A. The curves of the treated and untreated fibres followed the same pattern, and three curve parts could be distinguished. At low relative humidity (RH), up to approximatively 10 %, the water molecules were expected to bind to the surface of the sample in a monolayer by van der Waals forces. This involves the hydroxyl groups of hemicelluloses and amorphous cellulose as well as the carboxylic functions of pectin (Célino et al.

453 2014), all present in hemp fibre (Placet et al. 2017). Notice that for all samples, the

454 curves where the moisture content was below 10 %RH could be superimposed.
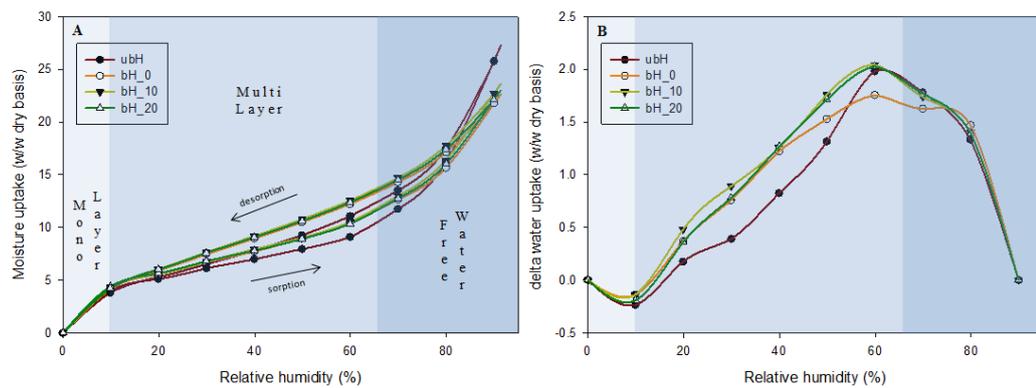


455

456

457 Figure 4: Sorption-desorption curve: moisture uptake expressed in percentage of dry matter (4A).

458 Hysteresis curve: delta moisture content (4B) as a function of relative humidity. The delta is the

459 subtraction of the moisture uptake in the desorption phase from the moisture uptake in the sorption

460 phase, at equivalent relative humidity.

461

462 When the entire surface was saturated, the molecules continued to adsorb and pile

463 up on the monolayer, forming a multilayer, until all accessible voids were filled.

464 Above approx. 65-70 %RH, water molecules aggregated in a free liquid state. At

465 relative humidity between 10 and 65 %, treated fibres adsorbed a greater quantity

466 of water than untreated fibres, meaning that the porous structure of the fibres had

467 opened, probably due to the extraction of some cell wall oligo-polysaccharides by

468 water-assisted mechanical removal, as shown by MIP. This was confirmed by

469 chemical analysis; see the next section. Thus, physical water sorption predominated

470 rather than chemo-sorption in this range, because although water absorbing

471 molecules (hemicelluloses/pectins) were extracted during treatment, more sorption

472 took place, which could be explained by mesoporosity overcompensation.

473 Regarding the isotherm curves of Figure 4A, at 90 % RH, untreated fibres

474 absorbed 25.7 % water compared to the 21-22 % moisture content of treated fibres.

475 The loop areas (Table 3) confirmed that the three treated fibres had a more

476 noticeable hysteresis response than the unbeaten fibres, with an area of 86.1, 94.4

477 and 91.7 $\omega$%·RH%, which were 15 %, 25 % and 22 % increases, for bH_0, bH_10

478 and bH_20, respectively. Thus, accessibility to sorption sites begins at the soaking

479 stage and is accentuated with mechanical treatment. In other words, hemp fibres

480 had a swelling capacity increased by beating, which seems to follow a similar

17

481  behaviour to that reported for lignocellulosic pulp (Pönni et al. 2012). This can

482  probably be connected to cell wall polymers water plastization and arguably by the

483  multiplication of defects (kink bands, fibrils…), where one could expect more

484  water-binding sites.

485  Even if isotherm curves had a similar trend (Figure 4A), the hysteresis curves

486  (Figure 4B) yielded more detail concerning the pore opening/closing mechanism

487  induced by mechanical treatment. At a relative humidity between 10 and 40 %, the

488  three treated fibres were almost superimposed and had a much higher adsorption

489  capacity than native fibres. Beyond that, the behaviour differed for bH_0 fibres,

490  since between 40 and 70 %, it adsorbed less water than bH_10 and bH_20 fibres

491  and even less than native fibres at RH between 55 and 70 %. From these

492  observations, we can deduce that water treatment opens smaller pores, unlike

493  hydro-mechanical treatment, which contributes to the opening of larger sites that

494  can adsorb water. Westenbroek (2000) mentioned that the small size of the lumen

495  makes the hemp fibres uncollapsible. However, the fact that the delta water content

496  of bH_0 was lower than that of native fibres between 55 and 70 % RH shows that

497  there was some closure of porous cavities.

498  Concerning the true density measured by DVS, all the sampled had a true density

499  between 1.53 and 1.55 g.cm$^{-3}$. The apparent skeletal density measured by MIP took

500  into account the internal porosity of the fibre, explaining that the measured density

501  was lower than true density, as recently explained by Legall et al. (2018) for flax

502  fibres. Because the apparent skeletal density of the most treated fibres in the bH_20

503  group was raised to 1.453 while the others decreased (1.28 for bH_0 and 1.25 for

504  bH_10) compared to untreated hemp fibres (1.38), no particular trend could be seen.

505  *Chemical composition*

506  To investigate chemical composition evolution due to treatment, an analysis of the

507  major dry matter based component of the hemp fibre was performed. The

508  polysaccharide, proteins and lignin contents were assessed (Figure 5A). The

509  untreated hemp fibres used in our study (ubH) were composed mainly of

510  polysaccharides, 86 % of the dry mass in total, including 75 % cellulose and 11 %

511  non-cellulosic polysaccharides (NCPs), which respectively corresponded to 87 %

512  and 13 % of the relative content of total polysaccharide. Additionally, the acid-

513  insoluble lignin fraction (called Klason lignin) represented 2.9 % of the dry matter,

514 similar to the protein content (3 %). These results of chemical composition of hemp

515 fibres are in agreement with those of the literature when comparable analytical

516 techniques were used (Crônier et al. 2005; Placet et al. 2017). Indeed, it is

517 noteworthy that the biochemical technique used here may give contrasting results

518 for the same sample.
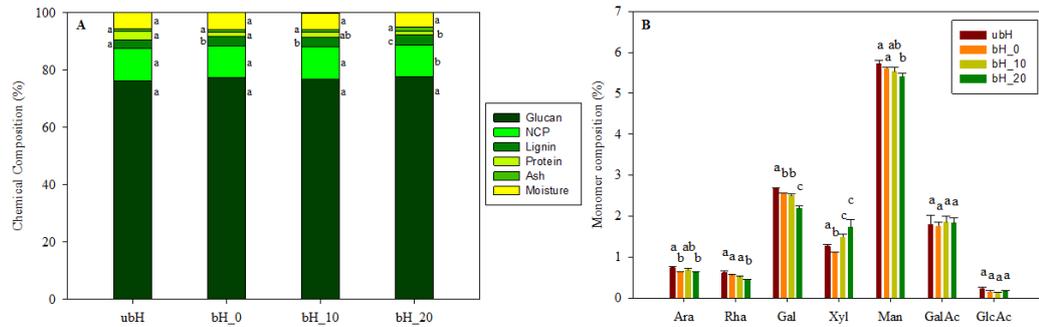
519



520 Figure 5: (A) Stacked bar charts of chemical composition expressed as the dry matter content. (B)

521 Monomer composition expressed as the percentage of total polysaccharide. Bars not having the

522 same letters are significantly different ($p < 0.05$).

523

524 When the fibres were soaked, the total sugar content slightly and gradually

525 increased with the mechanical treatment time, and finally became significantly

526 different at 20 minutes of beating (see Table 3). The opposite trend was observed

527 for proteins: from the soaking stage and up to 10 minutes of beating, their content

528 was significantly reduced by half to reach 1.4 % in 20 minutes of beating. In fact,

529 the aqueous suspension of hemp fibres caused the solubilization of proteins and

530 other low-molecular-weight organic compounds, furthering a slight enrichment of

531 cellulosic and phenolic fractions comparing to unbeaten hemp fibres (ubH). Some

532 proteins are located in the middle lamellae and primary cell walls and are arguably

533 water soluble. In contrast, another protein compartment is non-water soluble

534 because it interacts strongly with the cell wall network and directly with cellulose

535 microfibrils. Those are structural proteins and are generally glycoproteins from the

536 arabino-galactan protein superfamily, such as fasciclin-like arabinogalactan

537 proteins (Guerriero et al. 2017). Moreover, the peeling of the fibre cell wall by the

538 beating process increased the exchange surface with water and thus seemed

539 amplified this solubilization by removing more soluble components, letting more

540 polysaccharide polymers in the bH_20.

541 One would have expected the lignin to be extracted too, despite its low level in

542 hemp fibres but greater enrichment in the middle lamella due to its location.

543 However, its content evolved like the polysaccharide content. According to Akmar

544 et al. (2000), lignin can neither be modified nor extracted by simple mechanical

545 treatment such as the one we choose in this study.

546 We can see also that the relative proportion of the total non-cellulosic

547 polysaccharide fraction was not affected under the three conditions (Figure 5A).

548 However, looking in more detail at the monosaccharide composition of NCPs, the

549 repartition of some monomer units was slightly contrasted, depending on the

550 applied treatment. Arabinose, galactose and mannose units were significantly

551 declined by the soaking step. Then, when comparing the bH_0 with both beaten

552 samples, we can see first that the chemical composition of bH_10 was similar to

553 bH_0 except for xylose, which increased from 1.1 % to 1.5 % of total

554 polysaccharide. Under the most drastic treatment, bH_20, arabinose, rhamnose,

555 galactose, and mannose were reduced, possibly causing an enrichment of xylose.

556 The solubilization of these monomers, mainly inherent in the middle lamella and

557 the primary cell wall, facilitated the delamination of fibre bundles into unit fibres,

558 which is in line with the abovementioned diameter changes.

559 Additionally, special attention should be paid to the xylose content because in

560 contrast to the other NCPs components, it is the only one with an enriched content.

561 The quantified xylose in our study certainly could come from a xylan-rich layer

562 (located in the secondary cell wall), and the latter would not be affected by soaking

563 and beating. Interestingly, a xylose enrichment has also been reported during

564 bamboo processing by bleaching and caramelization procedures (Sharma et al.

565 2018); those authors hypothesized that the xylan backbone was covalently bonded

566 with other cell wall polymers, such as lignin via hydroxycinnamic moieties (such

567 as ferulic acids), to form a cross-linked network, which limited chemical access.

568 Galacturonic acid is often related to pectin, and in fruit it is often related to

569 rhamnogalacturonan I. Curiously, with hemp bast fibre elements, the level of

570 galacturonic acid was constant between all the conditions, suggesting that hemp

571 bast fibre pectin may have limited susceptibility to peeling treatment (Placet et al.

572 2017). Glucuronic and galacturonic acids were constant and not enriched, meaning

573 that they seemed removed, but the significance of this finding is questionable. To

574 close the polysaccharide examination, we have to recall that the processes used here

575  for our samples was unheated, non-alkaline and without barometric stress, leading

576  us to assume that this explains the relatively low rates of hemicelluloses and pectins

577  extracted from hemp fibres.

578  *Crystallinity of cellulose*

579  According to equation (1), the crystallinity index of untreated fibres (ubH) was 49.3

580  % (Table 3) which is in line with the expected values for hemp bast fibres (Dai and

581  Fan 2010; Shah 2013). The bH_0 sample had a crystallinity of 59.1 %, which

582  represented an increase in the index of 10 compared to ubH. Yao and co-workers

583  (Yao et al. 2018) have studied the hydro-thermal pretreatment effect on the structure

584  of corn stover cellulose and highlighted changes in cellulose conformation by

585  rearrangement of hydrogen bonds during decrystallisation-recrystallization phases

586  of cellulose occurring during pretreatment. Thus, possible polymer rearrangements

587  may have contributed to the increased crystallinity index, due to the water

588  environment and the closure of nanopores between the cellulose microfibrils, as

589  suggested by the porosity results above. A slight extraction of amorphous

590  components could increase the crystallinity index (Xu et al. 2013), but probably to

591  a lesser extent compared to the rearrangement of cellulose microfibrils.

592  The hydro-mechanical treatments resulted in a drop in the crystallinity index, index

593  values of 56.6 % and 54.1 % were obtained for bH_10 and bH_20, respectively.

594  Thus, mechanical treatment could have disrupted the crystalline structure of

595  microfibrils by inducing dislocations. These dislocation zones were defined as areas

596  of the fibre cell wall where the direction of the microfibrils (the angle of the

597  microfibrils) differed from the angle of the microfibrils of the surrounding cell wall

598  (Thygesen et al. 2006b). To support this hypothesis, Dai and Fan (2011) used FTIR

599  spectroscopy to quantify the crystallinity index of two kinds of hemp samples, one

600  without and the second with dislocations. They found that the crystallinity index

601  was 48.4 % for the hemp without dislocations and 41.3 % for those within

602  dislocation regions, showing a significant reduction in the crystallinity due to the

603  dislocations.

604  *Thermal stability evolution*

605  The evolution patterns of weight loss and their derivatives are shown in Figure 6.
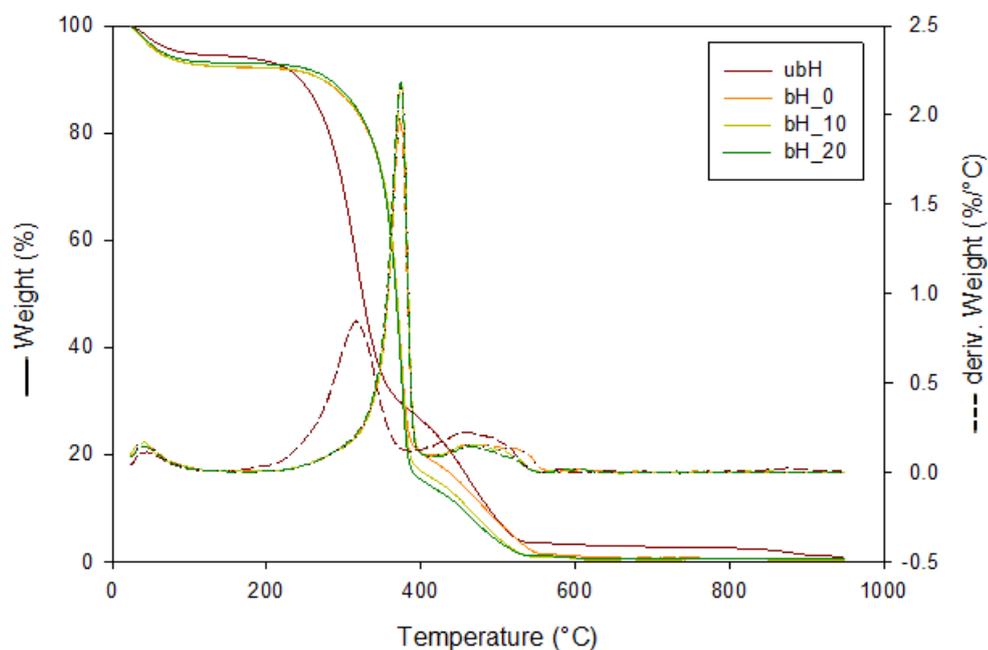
606

607 Figure 6: Thermogravimetric analysis curve. (-) percentage of weight and (---) derivative of weight
608 as degradation temperature (°C).

609

610 The decomposition steps of lignocellulosic biomasses have been extensively
611 studied (Carrier et al. 2011; Stefanidis et al. 2014). Even if the interactions between
612 hemicelluloses, cellulose and lignin are complex and have an impact on the thermal
613 stability of the samples, a common pattern emerges. Indeed after the dehydration
614 stage (peak I), the least stable compounds, pectins and hemicelluloses decomposed
615 between 210 and 350 °C, followed by cellulose (peak II) up to 400 °C. Pectins and
616 hemicelluloses having semi-crystalline polymers are often considered an
617 amorphous polymer *in planta*. Lignin is a more complex compound which is rich
618 in aromatic units and degrades at a high temperature, between 400-500 °C (peak
619 III), but starts slightly from 100 °C onwards, according to its condensation level. At
620 the end of the pyrolysis, what remains is called the ashes. The temperatures of
621 thermal degradation obtained are shown in Table 4 and are in agreement with the
622 above temperature ranges and those described in previous studies (Mazian et al.
623 2018).

624 Regarding the moisture content related to peak I (Table 4), we can note that fibres
625 contained similar moisture content.

626 Table 4: Thermogravimetric analysis peaks. Weight loss and mass residue (W%) expressed in
627 percentage and temperature (T°) expressed in °C.

| | Peak I | | Peak II | | Peak III | | Residue |
|---|---|---|---|---|---|---|---|
| | W% | T° | W% | T° | W% | T° | W% |
| ubH | 5.9 | 37.9 | 66.3 | 308.2 | 24.0 | 454.5 | 0.95 |
| | ± 0.35 | ± 5.0 | ± 0.47 | ± 0.62 | ± 0.37 | ± 0.2 | ± 0.07 |
| bH_0 | 5.8 | 39.5 | 74.9 | 362.7 | 17.2 | 484.4 | 0.59 |
| | ± 0.59 | ± 2.7 | ± 1.19 | ± 0.3 | ± 0.23 | ± 7.90 | ± 0.06 |
| bH_10 | 7 | 40.5 | 77.8 | 367.4 | 14.8 ± | 477.7 | 0.78 |
| | ± 0.94 | ± 0.01 | ± 0.1 | ± 6.79 | 0.15 | ± 6.08 | ± 0.13 |
| bH_20 | 6.0 | 38.5 | 79.9 | 361.8 | 13.0 | 457.6 | 0.6 |
| | ± 0.10 | ± 2.7 | ± 0.17 | ± 0.2 | ± 0.1 | ± 1.79 | ± 0.16 |

628

629 Additionally, the thermogravimetric analysis (Figure 6) shows that the cellulose
630 peak (peak II) was narrowed and shifted in the three treated fibres compared to the
631 untreated sample ubH. This could be explained by the extraction of water-soluble
632 components and thus higher cellulose crystallinity. The maximum temperature of
633 degradation of the cellulose (peak II) was 362.7 °C for the water-soaked fibres
634 against 308.2 °C for the raw fibres ubH, as shown in Figure 6, so it was necessary
635 to bring more thermal energy to degrade the cellulose. According to a study on
636 wood conducted by Giummarella et al. (2017), it would seem that the extraction of
637 hemicelluloses on the surface of cellulose microfibrils is in favour of stronger
638 interaction between lignin and cellulose. Even if hemp fibres have a lower lignin
639 content compared to wood, it is arguable that new interactions between
640 macromolecules of the cell wall involving cellulose were formed, resulting in a
641 higher thermostability, as shown experimentally in Figure 6, where we observed a
642 shift of temperature from 354.5°C to 484.4°C for hydro-treated fibres bH_10
643 compared to ubH at the maximum temperature of degradation of peak III. Then, we
644 can see that for bH_10 and bH_20, this temperature gradually decrease (477.7 and
645 457.6 °C) and simultaneously their percentage of weight loss also (14.8 and 13%).
646 The mass of degraded cellulose gradually increased from 66.3 % to 79.9 %,
647 confirming that the cellulose compartment was modified. At the end of pyrolysis,
648 the ash (residue) was less than 1 % for each sample.

649

650 *Mechanical properties by nanoindentation and correlation studies*

651 Nanoindentation tests were carried out to compare and discuss the impact of the
652 treatments on the stiffness of the hemp fibre cell walls (Table 3). It is important to
653 recall that with this technique, only the S2 sublayer, which is the most richly
654 cellulosic layer, can be reasonably investigated due to the small thickness of the
655 other sublayers. Due to the high mechanical anisotropy of hemp cell walls and
656 specific loading mode, nanoindentation can not clearly give absolute mechanical
657 data (Bourmaud and Baley 2009). Nevertheless, it is a suitable tool to compare
658 mechanical properties of plant cell walls, being the only method to obtain
659 mechanical information at the cell wall scale.

660 Untreated fibres had a 15.1 ±2.7 GPa indentation modulus, which, is in the same
661 range than literature data; for, example Marrot et al. (2013) measured indentation
662 modulus between 15.3 and 16.1 GPa in primary hemp fibres . However, this
663 stiffness started to drop as soon as the mechanical treatment was applied, decreasing
664 drastically to 11.2 ±1.0 and 8.4 ±1.0 GPa at 10 and 20 minutes of beating,
665 respectively, which made sense with the loss of crystallinity of cellulose.
666 Adusumalli (2014) also observed this decrease in cell wall nanoindentation stiffness
667 after bleaching and beating treatment on wood pulp fibres. Due to the solicitation
668 mode, the nanoindentation results are strongly impacted by the plant fibres MFA
669 (Jäger et al. 2011), the indentation modulus being particularly sensitive to cellulose
670 and the hardness to non-cellulosic polymer matrix. Indeed, the presence of
671 porosities in these latter may greatly impact the hardness, due to the calculation
672 method, which considers a theoretical contact area that may be false if the sample
673 is damaged, as it may have been here.

674 The decrease in the indentation modulus can also be attributed to an increase in
675 microfibrillar angle, as Tze et al. (2007) have shown for wood cell wall and as
676 Burgert and Keplinger (2013) mentioned in their review about nanomechanical
677 tests for plant cell walls. Once again, the loading mode is particularly sensitive to
678 macrofibrils stiffness but also to changes into MFA. In our case the important
679 increase into porosity content (Table 2) is in favour of changes into MFA values
680 and possible evolution of cell wall stiffness, as evidenced by nanoindentation
681 results.

682 Based on bibliographic data on the chemical composition (cellulose,
683 hemicelluloses, lignin, pectin, waxes) and physical properties (diameter, MFA,

24

length, density, moisture gain) of 21 types of natural fibres, Komuraiah et al. (2014) conducted a Pearson's correlation study to reveal the influence of these physicochemical characteristics on their macro-mechanical properties (tensile strength, specific strength, Young's modulus, specific Young's modulus, failure strain). Here, we applied this correlation test in an attempt to establish which chemical and structural modifications of the fibres undergoing mechanical treatment had the greatest impact on their indentation modulus, and to give additional data for the analyse and interpretation of mechanical tendencies noticed, correlation studies were carried out using Pearson's correlation test (Figure 7).
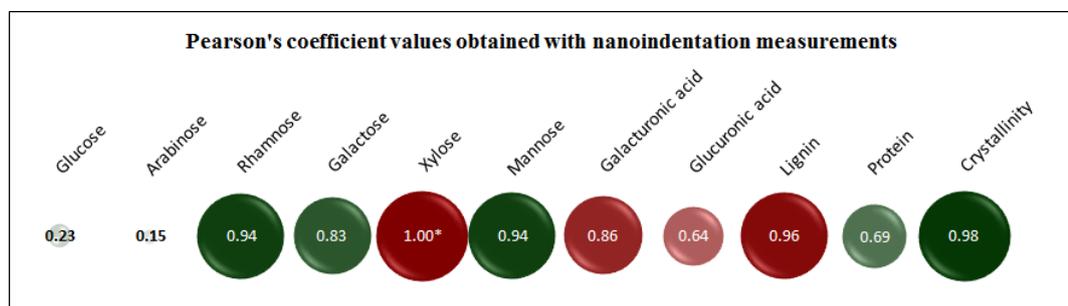


Figure 7: Pearson's correlation coefficient between nanoindentation measurements and treated fibre-related features. Disc diameter and colour shade display the strength of the correlation. Both positive and negative correlations are presented using the absolute value of the coefficients. Positive and negative correlations are displayed in green and red, respectively.

The mechanical properties, and especially the indentation modulus of the plant cell wall are mainly conferred by the cellulose microfibrils. Cellulose being a chain of glucose units, one would expect that the indentation modulus would be highly correlated with glucose content but also by properties and structure of cellulose. Here, the hydro-mechanical treatment applied to the fibres did not significantly impact the glucose content but gradually disorganizes the cellulose chains, causing both the crystallinity index and the indentation modulus to drop, these two parameters being strongly positively correlated (Figure 7). Moreover, the increase of porosity content within the cell wall is in favour of a drop of mechanical stiffness, especially due to the solicitation mode which may induce buckling of cellulose macrofibrils during indentation.

Interestingly, a strong correlation with the indentation modulus was obtained for rhamnose (0.94), galactose (0.83) and mannose (0.94), whereas these are mainly monomers composing pectins and hemicelluloses. In our study configuration, this

25

means that the indentation modulus decreased in proportion to the contents of these 3 non-cellulosic monomers. Pectins and hemicelluloses form a very complex network with microfibrils and act as a glue in this structure. Different authors have underlined the important function of non-cellulosic components into plant cell wall stiffness, favouring the link and cohesion between cellulose macrofibrils (Bourmaud and Baley 2009; Lefeuvre et al. 2015). Thus, the possible solubilization of such compounds may cause a relaxation of the microfibrils' structure, possibly resulting in an MFA rearrangement as well as a loss of cell walls mechanical properties.

One the other hand, xylose (1*) and lignin (0.96) had strong negative correlations with nanomechanical properties. In our case this shows a recalcitrance to extraction by water and the soft mechanical beating. Thus, the positive correlation noticed with nanoindentation modulus highlights the destructuration of cell walls and not the impact of these components on the mechanical performances. In our case, other monosaccharidic components such as Glucuronic acid (0.64) or arabinose (0.15) as well as proteins (0.69) are poorly correlated with mechanical properties of hemp cell walls; these components having lower structural function, compared to rhamnose or galactose for example. Due to indentation scale, which remains high compare to the parietal architecture one, and as discussed previously, a direct correlation between mechanical properties and components fraction can't be directly established but a global tendency is noticed. The increase into porosity ratio and the decrease into crystallinity degree and non-cellulosic polysaccharides are here the main contributors to the indentation stiffness decrease; they are responsible for a pronounced degradation of both parietal architecture and composition, inducing a drop into cell wall stiffness, which is especially pronounced due to the specific loading mode during an indentation test.

**Conclusion**

We explored the use of controlled hydro-mechanical fibre treatment processes, particularly beating, to modify the hemp fibre surface. Ultrastructural analysis revealed that beating led to fibre bundle individualisation and fibrillation; these account for the observed reduction in bundle diameter and densification of the fibre network, and subsequent increase in macroporosity and surface area, though

26

decreased nanoporosity. We expect these to enhance physical interactions between the fibres and the matrix for composite applications.

However, the beating treatment also influenced the fibres' biochemical properties. While initial hydro-treatment (soaking-drying) increased cellulose crystallinity substantially and extracted amorphous components such as pectins and hemicelluloses, subsequent beating cycles led to a drop in crystallinity probably due to defect formation.

The combination of changes in structural and biochemical properties led to the observed evolution in thermal, moisture absorption and nanomechanical properties. Specifically, thermal stability and water retention capacity improved with beating treatment. Indentation modulus increased upon hydro-treatment, but subsequently almost halved to 8.4 GPa after 20 mins of beating. A Pearson's correlation analysis determined that the indentation modulus was most correlated with cellulose crystallinity and the content of three non-cellulosic cell wall polysaccharides: rhamnose, galactose and mannose. The solubilisation of these polysaccharides may have reduced the microfibril angle.

## Acknowledgement

## Bibliography

Adusumalli RB, Passas R, Sreedhar I, Krishnamurthy B, Kombaiah B, Montagne A (2014) Nanoindentation of bleached and refined pulp fibres. IJMatEI 5:138-150. https://doi.org/10.1504/ijmatei.2014.060320

Akmar PF, Yusoff MNM, Kennedy JF, Knill CJ (2000) Compositional analysis of oil palm trunk fibers. In: Cellulosic Pulps, Fibres and Materials. Woodhead Publishing, pp 227-234

Andersons J, Spārniņš E, Poriķe E (2009) Strength and Damage of Elementary Flax Fibers Extracted from Tow and Long Line Flax. J Compos Mater 43:2653-2664. https://doi.org/10.1177/0021998309345035

Arnould O, Siniscalco D, Bourmaud A, Le Duigou A, Baley C (2017) Better insight into the nano-mechanical properties of flax fibre cell walls. Ind Crop Prod 97:224-228. https://doi.org/10.1016/j.indcrop.2016.12.020

Ausias G, Bourmaud A, Coroller G, Baley C (2013) Study of the fibre morphology stability in polypropylene-flax composites. Polym degrad Stabil 98:1216-1224. https://doi.org/10.1016/j.polymdegradstab.2013.03.006

Beaugrand J, Berzin F (2012) Lignocellulosic fiber reinforced composites: Influence of compounding conditions on defibrization and mechanical properties. J Appl Polym Sci 128:1227-1238. https://doi.org/10.1002/app.38468

Beaugrand J, Guessasma S (2015) Scenarios of crack propagation in bast fibers: Combining experimental and finite element approaches. Compos Struct 133:667 - 678. https://doi.org/10.1016/j.compstruct.2015.07.119

Beaugrand J, Guessasma S, Maigret J-E (2017) Damage mechanisms in defected natural fibers. Sci Rep-UK 7:14041. https://doi.org/10.1038/s41598-017-14514-6

Berzin F, Vergnes B, Beaugrand J (2014) Evolution of lignocellulosic fibre lengths along the screw profile during twin screw compounding with polycaprolactone. Compos Part A-Appl S 59:30-36. https://doi.org/https://doi.org/10.1016/j.compositesa.2013.12.008

Bourmaud A, Baley C (2009) Rigidity analysis of polypropylene/vegetal fibre composites after recycling. Polym degrad Stabil 94:297-305. https://doi.org/https://doi.org/10.1016/j.polymdegradstab.2008.12.010

Bourmaud A, Beaugrand J, Shah DU, Placet V, Baley C (2018) Towards the design of high-performance plant fibre composites. Pro Mater Sci 97:347-408. https://doi.org/10.1016/j.pmatsci.2018.05.005

Bourmaud A, Malvestio J, Lenoir N, Siniscalco D, Habrant A, King A, Legland D, Baley C, Beaugrand J (2017) Exploring the mechanical performance and in-planta architecture of secondary hemp fibres. Ind Crop Prod 108:1-5. https://doi.org/10.1016/j.indcrop.2017.06.010

Bourmaud A, Morvan C, Bouali A, Placet V, Perré P, Baley C (2013) Relationships between micro-fibrillar angle, mechanical properties and biochemical composition of flax fibers. Ind Crop Prod 44:343-351. https://doi.org/https://doi.org/10.1016/j.indcrop.2012.11.031

Burgert I, Keplinger T (2013) Plant micro- and nanomechanics: experimental techniques for plant cell-wall analysis. J Exp Bot 64:4635-4649. https://doi.org/10.1093/jxb/ert255

Carrier M, Loppinet-Serani A, Denux D, Lasnier J-M, Ham-Pichavant F, Cansell F, Aymonier C (2011) Thermogravimetric analysis as a new method to determine the lignocellulosic composition of biomass. Biomass Bioenerg 35:298-307. https://doi.org/https://doi.org/10.1016/j.biombioe.2010.08.067

Célino A, Fréour S, Jacquemin F, Casari P (2013) The hygroscopic behavior of plant fibers: a review. Front Chem 1:43. https://doi.org/10.3389/fchem.2013.00043

Célino A, Gonçalves O, Jacquemin F, Fréour S (2014) Qualitative and quantitative assessment of water sorption in natural fibres using ATR-FTIR spectroscopy. Carbohyd Polym 101:163-170. https://doi.org/10.1016/j.carbpol.2013.09.023

Chen M, Coasne B, Guyer R, Derome D, Carmeliet J (2018) Role of hydrogen bonding in hysteresis observed in sorption-induced swelling of soft nanoporous polymers. Nature Communications 9:3507. https://doi.org/10.1038/s41467-018-05897-9

Cheng Q, Wang J, McNeel J, Jacobson P (2010) Water retention value measurements of cellulosic materials using a centrifuge technique. Bioresources 5.

Chernova TE, Mikshina PV, Salnikov VV, Ibragimova NN, Sautkina OV, Gorshkova TA (2018) Development of distinct cell wall layers both in primary and secondary phloem fibers of hemp (Cannabis sativa L.). Ind Crop Prod 117:97-109. https://doi.org/https://doi.org/10.1016/j.indcrop.2018.02.082

Crônier D, Monties B, Chabbert B (2005) Structure and chemical composition of bast fibers isolated from developing hemp stem. J Agr Food Chem 53:8279-8289. https://doi.org/10.1021/jf051253k

Dai D, Fan M (2010) Characteristic and Performance of Elementary Hemp Fibre. Materials Sciences and Applications Vol.01No.06:4. https://doi.org/10.4236/msa.2010.16049

Dai D, Fan M (2011) Investigation of the dislocation of natural fibres by Fourier-transform infrared spectroscopy. Vibrational Spectroscopy 55:300-306. https://doi.org/https://doi.org/10.1016/j.vibspec.2010.12.009

Del Masto A, Trivaudey F, Guicheret-Retel V, Placet V, Boubakar L (2017) Nonlinear tensile behaviour of elementary hemp fibres: a numerical investigation of the relationships between 3D geometry and tensile behaviour. J Mater Sci 52:6591-6610. https://doi.org/10.1007/s10853-017-0896-x

Dienes D, Kemény S, Egyházi A, Réczey K (2005) Improving the capability of the Schopper–Riegler freeness measurement. Measurement 38:194-203. https://doi.org/https://doi.org/10.1016/j.measurement.2005.07.011

Dumas JBA (1831) Procédés de l'analyse organique. Annales de Chimie et de Physique:198-213.

Ferreira PJ, Matos S, Figueiredo MM (1999) Size Characterization of Fibres and Fines in Hardwood Kraft Pulps. Particle & Particle Systems Characterization 16:20-24. https://doi.org/10.1002/(sici)1521-4117(199905)16:1<20::aid-ppsc20>3.0.co;2-m

Gallos A, Paes G, Allais F, Beaugrand J (2017) Lignocellulosic fibers: a critical review of the extrusion process for enhancement of the properties of natural fiber composites. Rsc Adv 7:34638-34654. https://doi.org/10.1039/c7ra05240e

Gharehkhani S, Sadeghinezhad E, Kazi SN, Yarmand H, Badarudin A, Safaei MR, Zubir MNM (2015) Basic effects of pulp refining on fiber properties—A review. Carbohyd Polym 115:785-803. https://doi.org/10.1016/j.carbpol.2014.08.047

Giummarella N, Henriksson G, Salmén L, Laoko M (2017) On the effect of hemicellulose removal cellulose-lignin interactions. Nordic Pulp Paper Res J 32:542-549. https://doi.org/10.3183/NPPRJ-2017-32-04-p542-549

González López CV, García MdCC, Fernández FGA, Bustos CS, Chisti Y, Sevilla JMF (2010) Protein measurements of microalgal and cyanobacterial biomass. Bioresource Technol 101:7587-7591. https://doi.org/https://doi.org/10.1016/j.biortech.2010.04.077

Gourier C, Bourmaud A, Le Duigou A, Baley C (2017) Influence of PA11 and PP thermoplastic polymers on recycling stability of unidirectional flax fibre reinforced biocomposites. Polym degrad Stabil 136:1-9. https://doi.org/https://doi.org/10.1016/j.polymdegradstab.2016.12.003

Guerriero G, Mangeot-Peter L, Legay S, Behr M, Lutts S, Siddiqui KS, Hausman J-F (2017) Identification of fasciclin-like arabinogalactan proteins in textile hemp (Cannabis sativa L.): in silico analyses and gene expression patterns in different tissues. BMC Genomics 18:741. https://doi.org/10.1186/s12864-017-3970-5

Guessasma S, Beaugrand J (2019) Damage Kinetics at the Sub-micrometric Scale in Bast Fibers Using Finite Element Simulation and High-Resolution X-Ray Micro-Tomography. Front Plant Sci 10 https://doi.org/10.3389/fpls.2019.00194

Guicheret-Retel V, Cisse O, Placet V, Beaugrand J, Pernes M, Boubakar ML (2015) Creep behaviour of single hemp fibres. Part II: Influence of loading level, moisture content and moisture variation. J Mater Sci 50:2061-2072. https://doi.org/10.1007/s10853-014-8768-0

Herbaut M, Zoghlami A, Habrant A, Falourd X, Foucat L, Chabbert B, Paës G (2018) Multimodal analysis of pretreated biomass species highlights generic markers of lignocellulose recalcitrance. Biotechnol Biofuels 11:52. https://doi.org/10.1186/s13068-018-1053-8

Hill Callum AS, Norton A, Newman G (2009) The water vapor sorption behavior of natural fibers. J Appl Polym Sci 112:1524-1537. https://doi.org/10.1002/app.29725

Hughes M (2012) Defects in natural fibres: their origin, characteristics and implications for natural fibre-reinforced composites. J Mater Sci 47:599-609. https://doi.org/10.1007/s10853-011-6025-3

Jäger A, Hofstetter K, Buksnowitz C, Gindl-Altmutter W, Konnerth J (2011) Identification of stiffness tensor components of wood cell walls by means of nanoindentation.

Compos Part A-Appl S 42:2101-2109. https://doi.org/https://doi.org/10.1016/j.compositesa.2011.09.020

Komuraiah A, Kumar NS, Prasad BD (2014) Chemical Composition of Natural Fibers and its Influence on their Mechanical Properties. Mech Compos Mater 50:359-376. https://doi.org/10.1007/s11029-014-9422-2

Le Duigou A, Bourmaud A, Baley C (2015) In-situ evaluation of flax fibre degradation during water ageing. Ind Crop Prod 70:204-210. https://doi.org/https://doi.org/10.1016/j.indcrop.2015.03.049

Le Gall M, Davies P, Martin N, Baley C (2018) Recommended flax fibre density values for composite property predictions. Ind Crop Prod 114:52-58. https://doi.org/https://doi.org/10.1016/j.indcrop.2018.01.065

Le Moigne N, Otazaghine B, Stéphane C, Angellier-Coussy H, Anne B (2018) Surfaces and Interfaces in Natural Fibre Reinforced Composites. In: edn. Springer International Publishing.

Lee KY, Bismarck A (2014) 3 - Creating hierarchical structures in cellulosic fibre reinforced polymer composites for advanced performance. In: Hodzic A, Shanks R (ed) Natural Fibre Composites. Woodhead Publishing, pp 84-102

Lefeuvre A, Bourmaud A, Morvan C, Baley C (2014) Elementary flax fibre tensile properties: Correlation between stress–strain behaviour and fibre composition. Ind Crop Prod 52:762-769. https://doi.org/10.1016/j.indcrop.2013.11.043

Lefeuvre A, Duigou AL, Bourmaud A, Kervoelen A, Morvan C, Baley C (2015) Analysis of the role of the main constitutive polysaccharides in the flax fibre mechanical behaviour. Ind Crop Prod 76:1039-1048. https://doi.org/https://doi.org/10.1016/j.indcrop.2015.07.062

Legland D, Arganda Carreras I, Andrey P (2016) MorphoLibJ: integrated library and plugins for mathematical morphology with ImageJ. Bioinformatics 32:3532-3534. https://doi.org/10.1093/bioinformatics/btw413

Legland D, Beaugrand J (2013) Automated clustering of lignocellulosic fibres based on morphometric features and using clustering of variables. Ind Crop Prod 45:253-261. https://doi.org/10.1016/j.indcrop.2012.12.021

Liu M, Thygesen A, Summerscales J, Meyer AS (2017) Targeted pre-treatment of hemp bast fibres for optimal performance in biocomposite materials: A review. Ind Crop Prod 108:660-683. https://doi.org/10.1016/j.indcrop.2017.07.027

Marrot L, Lefeuvre A, Pontoire B, Bourmaud A, Baley C (2013) Analysis of the hemp fiber mechanical properties and their scattering (Fedora 17). Ind Crop Prod 51:317-327. https://doi.org/https://doi.org/10.1016/j.indcrop.2013.09.026

Mazian B, Bergeret A, Benezet J-C, Malhautier L (2018) Influence of field retting duration on the biochemical, microstructural, thermal and mechanical properties of hemp fibres harvested at the beginning of flowering. Ind Crop Prod 116:170-181. https://doi.org/10.1016/j.indcrop.2018.02.062

Meng X, Ragauskas AJ (2014) Recent advances in understanding the role of cellulose accessibility in enzymatic hydrolysis of lignocellulosic substrates. Curr Opin Biotech 27:150-158. https://doi.org/10.1016/j.copbio.2014.01.014

Mohanty AK, Vivekanandhan S, Pin J-M, Misra M (2018) Composites from renewable and sustainable resources: Challenges and innovations. Science 362:536.

Morvan C, Andème-Onzighi C, Girault R, Himmelsbach DS, Driouich A, Akin DE (2003) Building flax fibres: more than one brick in the walls. Plant physiol Bioch 41:935-944. https://doi.org/10.1016/j.plaphy.2003.07.001

Oliver WC, Pharr GM (1992) An improved technique for determining hardness and elastic modulus using load and displacement sensing indentation experiments. J Mater Res 7:1564-1583. https://doi.org/10.1557/jmr.1992.1564

Page DH (1989) The beating of chemical pulps–the action and the effects. In: Baker CF, Punton V (ed) Fundamentals of Papermaking, vol 1. Wiley, 9th Fundamental Research Symposium Notes, Cambridge, UK, pp 1-38

947    Pickering KL, Efendy MGA, Le TM (2016) A review of recent developments in natural
948          fibre composites and their mechanical performance. Compos Part A-Appl S 83:98-
949          112. https://doi.org/10.1016/j.compositesa.2015.08.038
950    Placet V, Day A, Beaugrand J (2017) The influence of unintended field retting on the
951          physicochemical and mechanical properties of industrial hemp bast fibres. J Mater
952          Sci 52:5759-5777. https://doi.org/10.1007/s10853-017-0811-5
953    Placet V, Méteau J, Froehly L, Salut R, Boubakar ML (2014) Investigation of the internal
954          structure of hemp fibres using optical coherence tomography and Focused Ion
955          Beam      transverse      cutting.      J      Mater      Sci      49:8317-8327.
956          https://doi.org/10.1007/s10853-014-8540-5
957    Pönni R, Vuorinen T, Kontturi E (2012) Proposed nano-scale coalescence of cellulose in
958          chemical pulp fibers during technical treatments. Bioresources 7.
959    Rask M, Madsen B, Sørensen BF, Fife JL, Martyniuk K, Lauridsen EM (2012) In situ
960          observations of microscale damage evolution in unidirectional natural fibre
961          composites.      Compos      Part      A-Appl      S      43:1639-1649.
962          https://doi.org/10.1016/j.compositesa.2012.02.007
963    ==Roux J-C, Bloch J-F, Bordin R, Nortier P (2009) The net normal force per crossing point==
964          ==: a unified concept for the low consistency refining of pulp suspensions.==
965          ==14th Fundamental Research Symposium: Advances in Pulp and Paper Research,==
966          ==FRC, Oxford, UK, pp. 51-83.==
967    Segal L, Creely JJ, Martin AE, Conrad CM (1959) An Empirical Method for Estimating
968          the Degree of Crystallinity of Native Cellulose Using the X-Ray Diffractometer.
969          Text Res J 29:786-794. https://doi.org/10.1177/004051755902901003
970    Shah DU (2013) Developing plant fibre composites for structural applications by
971          optimising composite parameters: a critical review. J Mater Sci 48:6083-6107.
972          https://doi.org/10.1007/s10853-013-7458-7
973    Shah DU, Nag RK, Clifford MJ (2016) Why do we observe significant differences between
974          measured and 'back-calculated' properties of natural fibres? Cellulose 23:1481-
975          1490. https://doi.org/10.1007/s10570-016-0926-x
976    Sharma B, Shah DU, Beaugrand J, Janeček E-R, Scherman OA, Ramage MH (2018)
977          Chemical composition of processed bamboo for structural applications. Cellulose.
978          https://doi.org/10.1007/s10570-018-1789-0
979    Stefanidis SD, Kalogiannis KG, Iliopoulou EF, Michailof CM, Pilavachi PA, Lappas AA
980          (2014) A study of lignocellulosic biomass pyrolysis via the pyrolysis of cellulose,
981          hemicellulose     and     lignin.     J     Anal     Appl     Pyrol     105:143-150.
982          https://doi.org/https://doi.org/10.1016/j.jaap.2013.10.013
983    Tanguy M, Bourmaud A, Beaugrand J, Gaudry T, Baley C (2018) Polypropylene
984          reinforcement with flax or jute fibre; Influence of microstructure and constituents
985          properties on the performance of composite. Compos Part B-Eng 139:64-74.
986          https://doi.org/10.1016/j.compositesb.2017.11.061
987    Thygesen A, Daniel G, Lilholt H, Thomsen AB (2006a) Hemp Fiber Microstructure and
988          Use of Fungal Defibration to Obtain Fibers for Composite Materials. J Nat Fibers
989          2:19-37. https://doi.org/10.1300/J395v02n04_02
990    Thygesen LG, Bilde-Sørensen JB, Hoffmeyer P (2006b) Visualisation of dislocations in
991          hemp fibres: A comparison between scanning electron microscopy (SEM) and
992          polarized     light     microscopy     (PLM).     Ind     Crop     Prod     24:181-185.
993          https://doi.org/https://doi.org/10.1016/j.indcrop.2006.03.009
994    Turner S, Kumar M (2018) Cellulose synthase complex organization and cellulose
995          microfibril structure. Philos Trans A Math Phys Eng Sci 376 2112. https://doi.org/
996          10.1098/rsta.2017.0048.
997    Tze WTY, Wang S, Rials TG, Pharr GM, Kelley SS (2007) Nanoindentation of wood cell
998          walls: Continuous stiffness and hardness measurements. Compos Part A-Appl S
999          38:945-953. https://doi.org/https://doi.org/10.1016/j.compositesa.2006.06.018

Wambua P, Ivens J, Verpoest I (2003) Natural fibres: can they replace glass in fibre reinforced plastics? Compos Sci Technol 63:1259-1264. https://doi.org/10.1016/S0266-3538(03)00096-4

Wang B, Sain M, Oksman K (2007) Study of Structural Morphology of Hemp Fiber from the Micro to the Nanoscale. Appl Compos Mater 14:89. https://doi.org/10.1007/s10443-006-9032-9

Washburn EW (1921) The Dynamics of Capillary Flow. Phys Rev 17:273-283. https://doi.org/10.1103/PhysRev.17.273

Westenbroek A (2000) Extrusion pulping of natural fibres. Universiteit of Twente

Xu F, Shi Y-C, Wang D (2013) X-ray scattering studies of lignocellulosic biomass: A review. Carbohyd Polym 94:904-917. https://doi.org/https://doi.org/10.1016/j.carbpol.2013.02.008

Yao K, Wu Q, An R, Meng W, Ding M, Li B, Yuan Y (2018) Hydrothermal pretreatment for deconstruction of plant cell wall: Part II. Effect on cellulose structure and bioconversion. Aiche J 0. https://doi.org/10.1002/aic.16106

Zhong LX, Fu SY, Zhou XS, Zhan HY (2011) Effect of surface microfibrillation of sisal fibre on the mechanical properties of sisal/aramid fibre hybrid composites. Compos Part A-Appl S 42:244-252. https://doi.org/https://doi.org/10.1016/j.compositesa.2010.11.010